Int. J. Electron. Commun. (AEÜ) 168 (2023) 154674

Contents lists available at ScienceDirect

Int. J. Electron. Commun. (AEÜ)

journal homepage: www.elsevier.com/locate/aeue

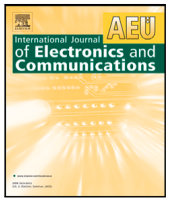

Regular paper

An improved pedestrian dead reckoning algorithm based on smartphone built-in MEMS sensors

Guiling Zhao *, Xu Wang, Hongxing Zhao, Zihao Jiang

School of Geomatics, Liaoning Technical University, Fuxin 123000, China

ARTICLE INFO

Keywords:
Smartphone
Indoor positioning
PDR
Dual-feature
Three-steps constraint
ADE

ABSTRACT

With the advantages of low cost, small size and lightweight, the smartphone has played a more and more important role in pedestrian indoor positioning. In particular, the application of Pedestrian Dead Reckoning (PDR) in the smartphone built-in MEMS sensors makes the application of smartphone more extensive. However, the zero-bias instability of the smartphone built-in MEMS sensors leads to the rapid accumulation of pedestrian trajectory calculation error. To solve this problem, we used the bias drift model and Kalman filter (KF) to denoise the original MEMS data. The dual-feature step detection model of peak domain and time domain was established to provide accurate step information for step length estimation and heading correction. Based on the Weinberg model, the three-steps constraint step length estimation (TCSLE) model was proposed to estimate step length accurately. Then, based on the improved heuristic drift elimination (iHDE), the adaptive drift elimination (ADE) model was proposed to identify different walking states. The correction models under different walking states were established to correct the heading angle accurately. Finally, the pedestrian trajectory was reconstructed using accurate step length and heading information. To verify the performance of the PDR algorithm based on the above model, three experimenters with different heights and genders were recruited, and three mobile phones with different sensor performance were selected. The experimenters moved smoothly and steadily with hand-held mobile phone, and 18 sets of experiments were carried out along two paths. The experiment results shown that the step length deviation was less than 1.4871 %, the horizontal positioning error was less than 1.6070 m, and the relative positioning error was less than 1.1816 %D. The proposed PDR algorithm has strong adaptability and robustness, and meets the needs of pedestrian indoor positioning.

1. Introduction

In recent years, with the rapid development of mobile internet, the smartphone has become the main source of information acquisition and plays a more and more important role in pedestrian indoor navigation and positioning [1,2]. At present, the smartphone is equipped with various built-in sensors, such as accelerometer, gyroscope, electronic compass, magnetometer, GNSS receiver, etc [3,4]. Among these sensors, GNSS receiver can provide users with accurate navigation and positioning information in outdoor scenarios with good signals [5,6]. However, In indoor and tunnel environments with poor signals, GNSS receiver cannot accurately locate due to signal blocking, multipath, non-line-of-sight and other effects [7,8].

In order to meet the needs of pedestrian indoor navigation and positioning, indoor positioning technologies based on smartphone are constantly being researched and developed. Among them, some indoor positioning technologies such as Bluetooth Low Energy (BLE) [9, 10], Wi-Fi [11–13], Magnetic Matching (MM) [14], Received Signal Strength (RSS) [15], and Radio Frequency Identification (RFID) [16] rely on the internal infrastructure of the building, and they need to build the corresponding database inside the building in advance. The smartphone built-in MEMS sensors can reconstruct the pedestrian trajectory by acquiring inertial data. However, due to the poor performance of MEMS and the low quality of IMU measurement information, the classical SINS algorithm is no longer applicable [17–19]. The PDR algorithm based on pedestrian gait updates pedestrian position by processing sensor measurement information, and it has good application prospects and feasibility [20–22]. PDR includes step detection, step length estimation, and heading correction [23–26]. Among them, the step length estimation and heading correction are greatly affected by the zero-bias instability of the smartphone built-in MEMS sensors. The step length error and heading error accumulate continuously, and the pedestrian trajectory error diverges with time [27–29]. Therefore, the

* Corresponding author.
E-mail address: zhaoguiling@lntu.edu.cn (G. Zhao).

https://doi.org/10.1016/j.aeue.2023.154674
Received 19 January 2023; Accepted 19 April 2023
Available online 29 April 2023

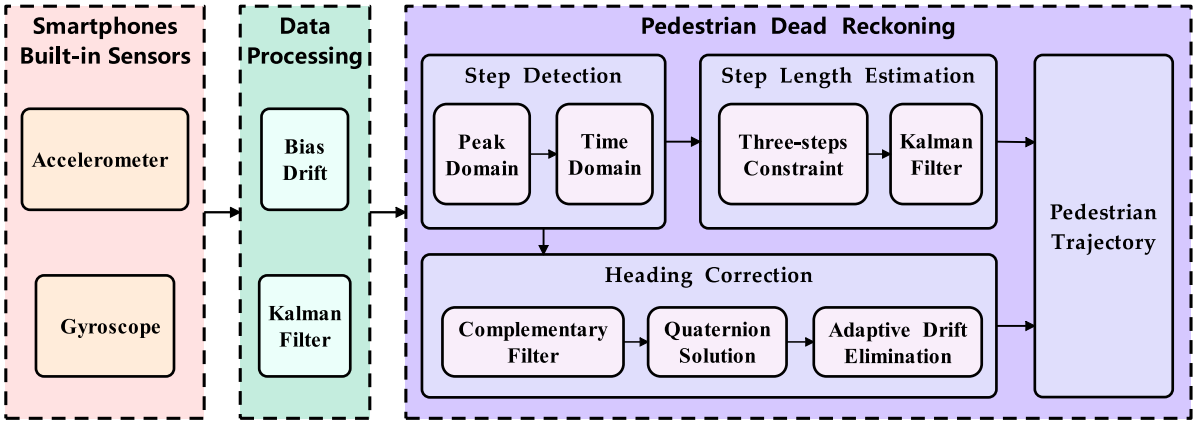

Fig. 1. The flowchart of PDR algorithm.

accuracy of step length estimation and heading correction restricts the accuracy of PDR algorithm.

For the study of step length estimation, the traditional step length estimation models include Weinberg model, Scarlet model, Kim model, linear model and so on. Xu et al. [30] constructed an improved step length estimation model based on surface electromyogram (EMG) signals, and used the characteristic parameters of surface EMG signals and step information to estimate step length accurately. However, the model parameters are set strictly and have certain limitations. Yao et al. [31] added the variance of acceleration and step information to the Weinberg model to estimate the step length adaptively. However, the relative positioning error is high, reaching 3%D. Hannink et al. [32] trained a deep convolutional neural network (CNN) to map stridespecific inertial sensor data to the final stride length. Based on the Weinberg and Kim models, Vezouznik et al. [33] used principal component analysis to characterize the relationship between step length and human kinematics. However, both deep CNN and principal component analysis need to collect a large amount of data for training. These algorithms are more complex, which greatly improve the operation cost.

For the study of heading correction, the commonly used heading correction methods include complementary filter (CF), zero velocity update (ZUPT), heuristic drift elimination (HDE), deep learning and so on. Zhang et al. [34] established a CF model, and the electronic compass output was used to constrain the heading angle calculated by the quaternion solution so as to obtain accurate heading information. However, when the pedestrian turns, the heading correction effect is not good. Wang et al. [35] proposed a HDE algorithm based on buffer zone. The algorithm adjusted the correction coefficient of heading angle in time to avoid overcorrection. However, the main direction is set less so that it is difficult to describe the more complex indoor environment. Hu et al. [36] proposed a high-precision magnetic-assisted heading angle calculation method based on a 1D convolutional neural network (CNN) in a Complicated Magnetic Environment. A team from the University of Toronto Institute for Aerospace Studies [37] explored robust inertial navigation using Long Short-Term Memory (LSTM) to improve the accuracy of inertial navigation systems. However, both 1D-CNN and LSTM need to collect a large amount of data for training. These algorithms are more complex, which greatly improve the operation cost.

To solve the above problems, we propose a PDR algorithm based on three-steps constraint step length estimation (TCSLE) and adaptive drift estimation (ADE). The contributions of this paper are summarized as follows:

- Bias drift model and Kalman filter (KF) are used to denoise the original MEMS data. A dual-feature step detection model based on the peak domain and time domain is established to provide accurate acceleration, angular velocity and step information for step length estimation and heading correction.
- In order to suppress the step length error, based on the Weinberg model, the TCSLE model is established by valuing the proportion of the three steps in front of the current step. Then KF is used to estimate the current step length accurately.
- In order to suppress the heading error, a CF model is established to correct the angular velocity, and then the heading angle is calculated by quaternion. Based on the improved heuristic drift elimination (iHDE) model, the adaptive drift elimination (ADE) model is proposed to identify different walking states and correct heading accurately.

The remainder of this paper is organized as follows: Section 2 is the PDR algorithm and data preparation. In Section 3, the main proposed models are introduced, including TCSLE and ADE models. Section 4 describes the experiment and discusses the experimental results in detail. We present conclusions of the paper and reveal some future works in Section 5.

2. PDR algorithm and data preparation

PDR is an important pedestrian indoor positioning technology. Through the original data such as acceleration and angular velocity collected by the smartphone built-in MEMS sensors, the pedestrian step length and heading angle are calculated to determine the pedestrian trajectory. PDR algorithm is defined as follows [38]:

$$\begin{cases} X_k = X_{k-1} + L_k \sin(\varphi_k) \\ Y_k = Y_{k-1} + L_k \cos(\varphi_k) \end{cases} \tag{1}$$

Where (X_{k-1}, Y_{k-1}) represents the position of step $k-1$; L_k and φ_k represent the step length and heading angle of step k, respectively; (X_k, Y_k) represents the position of step k.

According to Eq. (1), the focus of reconstructing pedestrian trajectory is to calculate the step length and heading angle. The flowchart of PDR algorithm is shown in Fig. 1.

Part 1 is the data processing. Bias drift and KF are used to denoise the original data, providing accurate acceleration and angular velocity information for Parts 2, 3 and 4. This process is introduced in detail in Section 2.1.

Part 2 is the step detection. The peak domain and time domain are set for dual-feature step detection to provide step information for Parts 3 and 4. This process is introduced in detail in Section 2.2.

Part 3 is the step length estimation. The three steps in front of the current step are valued the proportion to constraint step length. Then the TCSLE model combinates with KF to accurately estimate the current step length. This process is introduced in detail in Section 3.1.

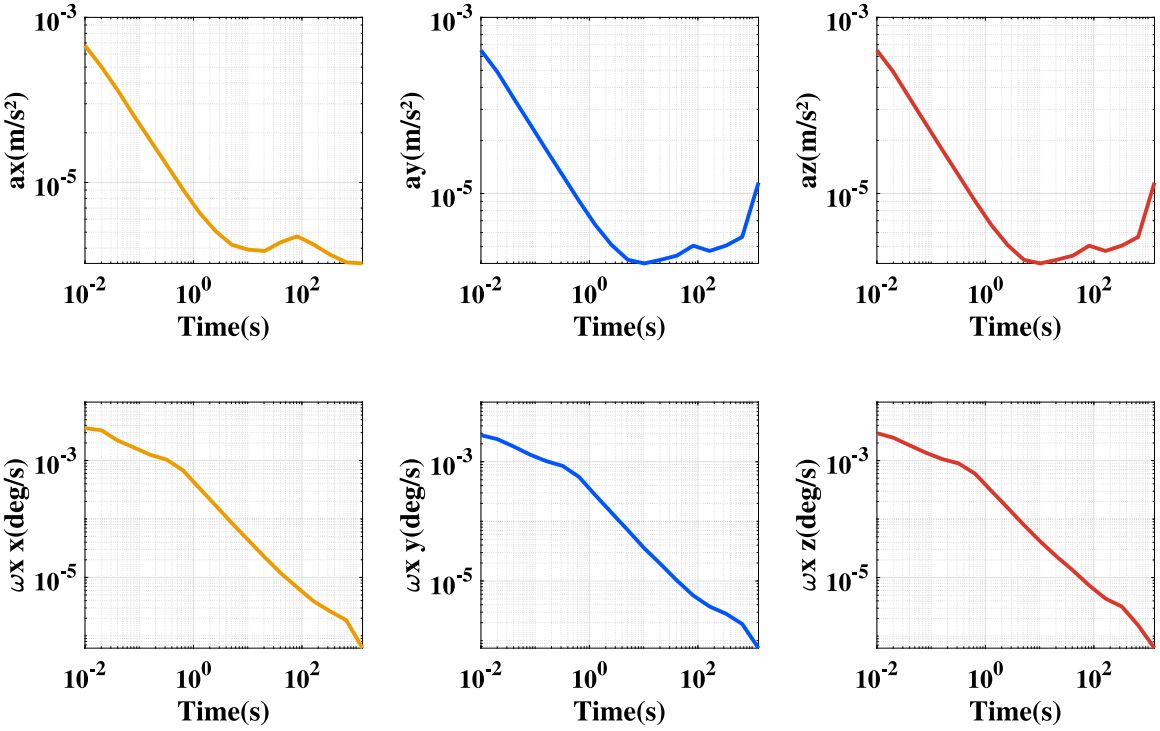

Fig. 2. The Allan standard deviation double logarithmic curve.

Part 4 is the heading correction. The CF model is established to correct the angular velocity, and the heading angle is calculated by quaternion solution. Then the ADE model is established to accurately correct the heading angle. This process is introduced in detail in Section 3.2.

Part 5 uses the step length and heading angle obtained in Parts 3 and 4 to reconstruct the pedestrian trajectory.

2.1. Data processing

The step length estimation and heading correction are easily affected by the zero-bias instability of the smartphone built-in MEMS sensors, and the step length error and heading error accumulate with time. These problems will cause the pedestrian trajectory error to diverge gradually. Therefore, accurate acceleration, angular velocity and step information are needed for estimating step length and correcting heading. In this paper, Allan variance analysis [39–41] is used to analyze the static error indexes of the smartphone built-in accelerometer and gyroscope.

The static outputs of an hour's smartphone built-in accelerometer and gyroscope are collected, and the Allan standard deviation double logarithmic curve is calculated as shown in Fig. 2.

It can be seen from Fig. 2 that the first half slope of the accelerometer three-axis Allan standard deviation is close to $-1/2$, and the second half slope is close to 0. Then the accelerometer has random noise error and bias error. The slope of the gyroscope three-axis Allan standard deviation is close to $-1/2$, and then the gyroscope has random noise error. Therefore, it is necessary to build different error processing models to pre-process the static error of smartphone built-in MEMS sensors.

2.1.1. Bias drift

For the bias error of smartphone built-in MEMS sensors, we establish the bias drift model for processing. Taking the processing of accelerometer bias error as an example, the three-axis static output of smartphone built-in accelerometer is collected, and the average values of three-axis acceleration axn, ayn and azn (n is the number of acquisition) are calculated. In the static state, the three-axis ideal output of the smartphone built-in accelerometer is $[0\ 0\ g]^T$. The three-axis bias error of the smartphone built-in accelerometer can be obtained by averaging the accelerometer static output.

$$\begin{cases} \bar{a}_x = (a_{x1} + a_{x2} + \cdots + a_{xn})/n \\ \bar{a}_y = (a_{y1} + a_{y2} + \cdots + a_{yn})/n \\ \bar{a}_z = (a_{z1} + a_{z2} + \cdots + a_{zn})/n - g \end{cases} \tag{2}$$

The static output of smartphone built-in accelerometer and gyroscope is collected. The local gravity acceleration is known as: $g = 9.78049$, then the three-axis bias error can be calculated by Eq. (2). The results are shown in Table 1.

Table 1
The bias error of smartphone built-in MEMS sensors.

a_x (m/s^2)	a_y (m/s^2)	a_z (m/s^2)	$\omega_x(10^{-5}$ rad/s)	$\omega_y(10^{-5}$ rad/s)	$\omega_z(10^{-5}$ rad/s)
0.0741	0.1952	0.0581	1.5904	0.2448	2.6944
0.4492	0.1075	−0.0176	47.8434	−18.3544	−11.6426
0.1040	0.1906	0.0582	−4.9262	4.5468	3.2504
0.1021	0.1922	0.0595	−3.4265	7.4110	−1.0118
0.0899	0.1840	0.0617	−0.0007	1.0324	3.5108
0.1639	0.1739	0.0440	8.2161	−1.0239	−0.6398

It can be seen from Table 1 that the bias error of the smartphone built-in accelerometer is $[0.1639\ 0.1739\ 0.0440]^T$ m/s^2, and the bias error of the smartphone built-in gyroscope is $[8.2161\ -1.0239\ -0.6398]^T$ 10^{-5} rad/s. Then the experimental data are processed by the bias error.

2.1.2. Kalman filter

For the random noise of the smartphone built-in MEMS sensors, we use KF to process it. KF is an algorithm to estimate system state optimally by using system observation data [42–44]. Taking the processing of gyroscope random noise as an example, the KF model is established by setting the system observation value as ω and the system state as Ω:

$$\begin{cases} K_k = P_{k|k-1}/(P_{k|k-1} + R) \\ \Omega_{k|k} = \Omega_{k-1|k-1} + K_k * (\omega_k - \Omega_{k-1|k-1}) \\ P_{k+1|k} = (1 - K_k) * P_{k|k-1} + Q \end{cases} \tag{3}$$

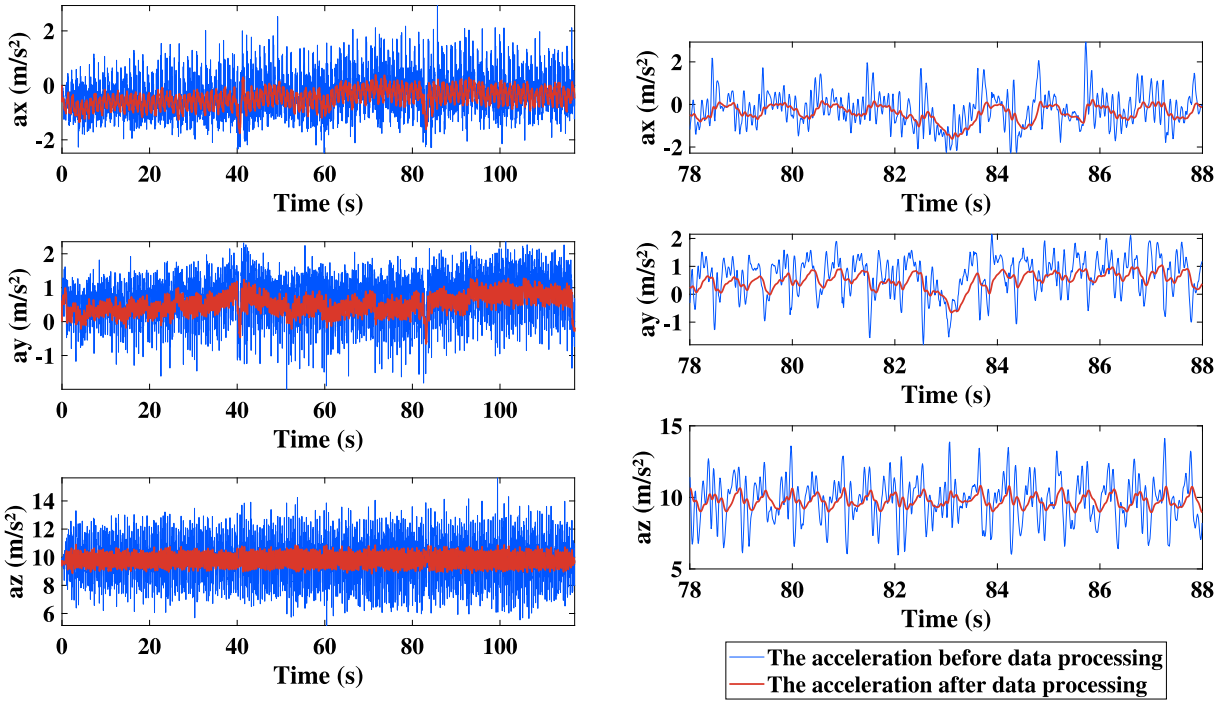

Fig. 3. The acceleration after data processing.

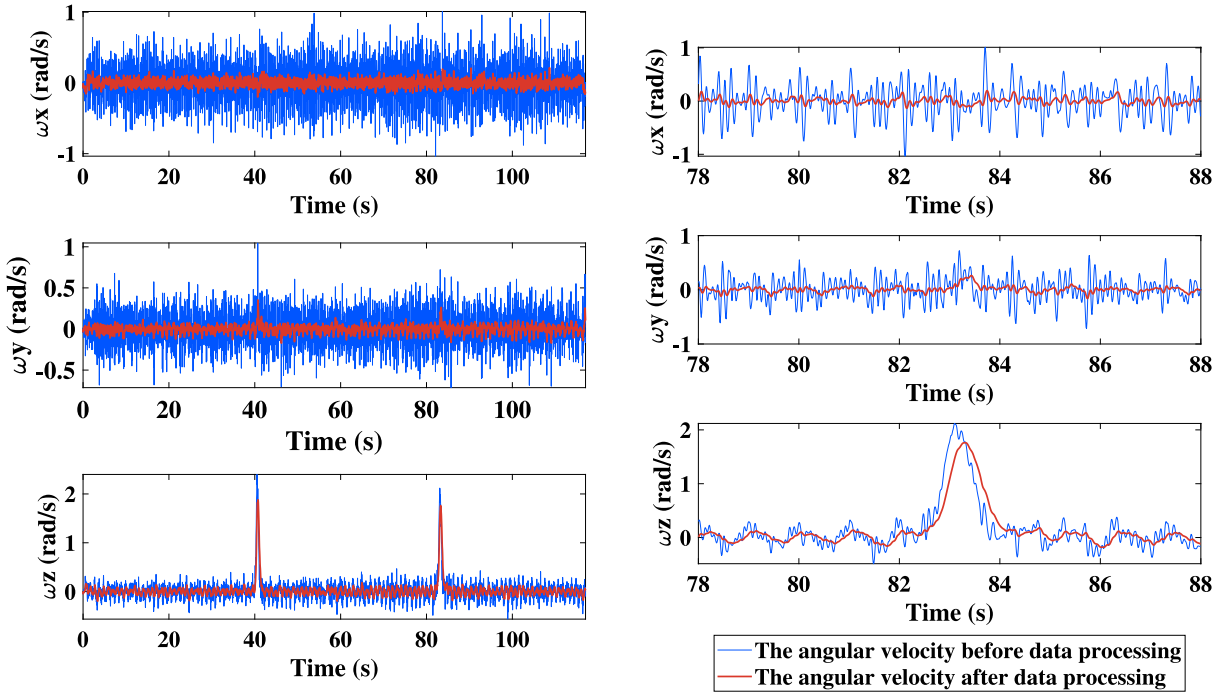

Fig. 4. The angular velocity after data processing.

Where K represents the Kalman gain; P represents the error covariance; R and Q represent the noise covariance. Through the bias drift and KF, accurate acceleration and angular velocity information can be obtained. The data preprocessing results are shown in Figs. 3 and 4.

In Figs. 3 and 4, the left side is the full three-axis acceleration and angular velocity curve. The right side is the three-axis acceleration and angular velocity curve from 78 s to 88 s. The period of time includes different walking states, such as straight, straight change to turn, turn

Table 2
The step detection results.

Experimental serial number	Smartphone brand	Velocity	Number of detection steps	Accuracy (%)
1	XIAOMI 11 Pro	Fast	228	100
2			229	99.6
3		Slow	231	98.7
4			229	99.6
5	HUAWEI Enjoy 10 Plus	Fast	228	100
6			229	99.6
7		Slow	231	98.7
8			229	99.6
9	HUAWEI MATE 30	Fast	228	100
10			229	99.6
11		Slow	231	98.7
12			229	99.6

and so on. It can be seen from Figs. 3 and 4 that after data preprocessing, the acceleration and angular velocity are not only improved, but also retains the original information. At the same time, we can find that a_x, a_y, ω_z appear larger fluctuations, when the experimenter turns in 40 s and 83 s.

2.2. Step detection

Because of the influence of the external environment, sensors' accuracy, pedestrian body shaking and so on, in addition to the real step point, the pseudo-peak will be judged as the step point. Therefore, based on the peak detection, we use the dual-feature detection of peak domain and time domain to constrain the step point jointly.

(1) Feature 1: peak domain

When the pedestrian walks normally, the resultant acceleration peak will have a threshold A. The size of A varies from person to person and is set according to the actual situation. Only when the resultant acceleration peak exceeds A will it be judged as the step point, the judging condition is expressed as follow:

$$\begin{cases} a_p(k) > A \\ a_f = a_p(k) \end{cases} \tag{4}$$

Where $a_p(k)$ represents the resultant acceleration peak in the time of k; a_f represents the step point obtained by the peak domain constraint.

(2) Feature 2: time domain

Although the peak domain can eliminate some pseudo-peaks, the other pseudo-peaks still satisfy Eq. (4). Therefore, based on the peak domain, the time domain is used to judge the step point again.

When the pedestrian walks normally, there is an interval $[t_{\min}\ t_{\max}]$ between two adjacent step points, and the interval size is set according to the actual step frequency. Only when the time interval is in $[t_{\min}\ t_{\max}]$, the larger peak point in the two adjacent step points will be judged as the step point, the judging condition is expressed as follow:

$$\begin{cases} t_{\min} < \Delta t_{k-1|k} < t_{\max} \\ a_{ff} = \max(a_f(k), a_f(k-1)) \end{cases} \tag{5}$$

Where $\Delta t_{k-1|k}$ represents the time interval from $k-1$ to k; $a_f(k)$ and $a_f(k-1)$ represent the step points obtained by peak domain constraint, respectively; a_{ff} represents the step point obtained by time domain constraint.

Accurate step information can be obtained by dual-feature step detection. Twelve groups' experiments are performed using different smartphones and walking speeds. The actual step numbers are 228. The step detection results are shown in Table 2.

It can be seen from Table 2 that the accuracy of step detection can reach more than 99%. Taking Experiment 1 as an example, the step detection result is shown in Fig. 5.

Through data processing and step detection in Sections 2.1 and 2.2, accurate acceleration, angular velocity and step information are obtained. Then the information provides the initial data for the TCSLE and ADE models proposed in Section 3 to reconstruct accurate pedestrian trajectory.

3. The proposed step length estimation and heading correction models

3.1. Three-steps constriant step length estimation model

The smartphone built-in MEMS sensors have low accuracy. The displacement obtained by using the inertial navigation algorithm alone has data drift, and the error accumulates with time. Therefore, based on the Weinberg model, we add three-steps constraint and KF to improve the accuracy of step length estimation. Based on the nonlinear relationship between the step length and the acceleration amplitude, the Weinberg model is defined as follows:

$$l = K * \sqrt[4]{a_{\max} - a_{\min}} \tag{6}$$

Where K represents the step length estimation coefficient, and it is obtained by training; $a_{\max}$ and $a_{\min}$ represent the maximum and minimum values of resultant acceleration in a single step, respectively.

The three steps in front of the current step are given the proportion, then the step length estimation model is expressed as follows:

$$l_i = q * (l_{i-1} + l_{i-2} + l_{i-3})/3 + (1-q) * K * \sqrt[4]{a_{\max} - a_{\min}} \tag{7}$$

Where q represents the proportion coefficient of the three steps in front of the current step, and it is valued as 0.6; l_{i-1}, l_{i-2}, l_{i-3} represent the three steps length in front of the current step, respectively.

Improve step accuracy with KF:

$$\begin{cases} K_k = P_{k|k-1}/(P_{k|k-1} + R) \\ L_{k|k} = L_{k-1|k-1} + K_k * (l_k - L_{k-1|k-1}) \\ P_{k+1|k} = (1 - K_k) * P_{k|k-1} + Q \end{cases} \tag{8}$$

Where l represents the system observation value; L represents the system state quantity; the meanings of P, K and Q are the same as Eq. (3).

3.2. Adaptive drift estimation model

Euler angle algorithm, direction cosine algorithm, quaternion algorithm and Rodrigues parameter algorithm are often used to solve the attitude angle. Among them, the quaternion algorithm has the advantages of high precision, low complexity and avoidable singularity, which can better optimize the heading. Therefore, this paper describes the pedestrian attitude information by quaternion. In order to reduce the gyroscope drift error and improve the heading accuracy, we establish the CF model, and uses the three-axis output of the smartphone built-in accelerometer to correct the angular velocity. The CF model is expressed as follows:

$$\begin{bmatrix} \omega_x \\ \omega_y \\ \omega_z \end{bmatrix} = \begin{bmatrix} \omega_x \\ \omega_y \\ \omega_z \end{bmatrix} + k_f \begin{bmatrix} 0 & -a_z & a_y \\ a_z & 0 & -a_x \\ -a_y & a_x & 0 \end{bmatrix} * \begin{bmatrix} 2(q_1q_3 - q_0q_2) \\ 2(q_2q_3 + q_0q_1) \\ 1 - 2(q_1^2 + q_2^2) \end{bmatrix}$$

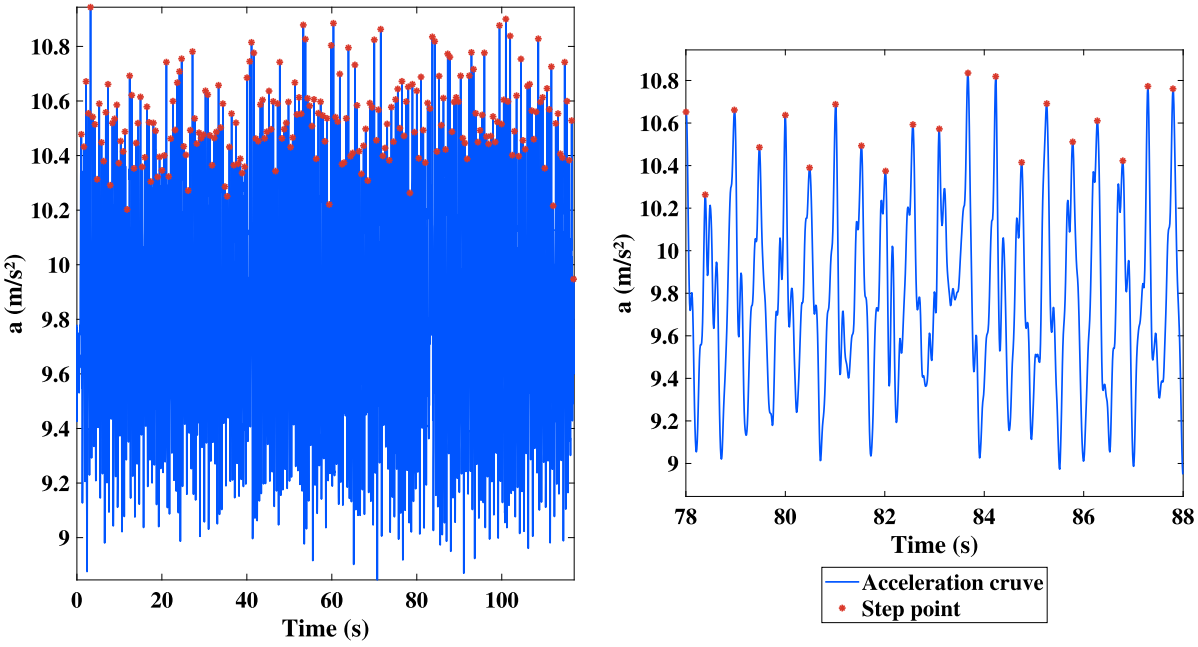

Fig. 5. The result of step detection.

$$+\sum k_e * dt * \begin{bmatrix} 0 & -a_z & a_y \\ a_z & 0 & -a_x \\ -a_y & a_x & 0 \end{bmatrix} * \begin{bmatrix} 2(q_1q_3 - q_0q_2) \\ 2(q_2q_3 + q_0q_1) \\ 1 - 2(q_1^2 + q_2^2) \end{bmatrix} \quad (9)$$

Where $[\omega_x\ \omega_y\ \omega_z]^T$ represents the three-axis output of the smartphone built-in gyroscope; k_f represents the correction coefficient, and it is valued as 0.8; $[a_x\ a_y\ a_z]^T$ represents the normalized three-axis output of the smartphone built-in accelerometer; $[q_0\ q_1\ q_2\ q_3]^T$ represents the initial quaternion $[1\ 0\ 0\ 0]^T$; ke represents the error integral coefficient, and it is valued as 0.1; dt represents the period, and it is valued as 0.01.

Update the quaternion using the first-order Runge–Kutta algorithm:

$$\begin{bmatrix} q_0 \\ q_1 \\ q_2 \\ q_3 \end{bmatrix} = \begin{bmatrix} q_0 \\ q_1 \\ q_2 \\ q_3 \end{bmatrix} + \frac{dt}{2} \begin{bmatrix} 0 & -\omega_x & -\omega_y & -\omega_z \\ \omega_x & 0 & \omega_z & -\omega_y \\ \omega_y & -\omega_z & 0 & \omega_x \\ \omega_z & \omega_y & -\omega_x & 0 \end{bmatrix} * \begin{bmatrix} q_0 \\ q_1 \\ q_2 \\ q_3 \end{bmatrix} \quad (10)$$

The smartphone built-in sensors frame is defined as aligning to the local east, north and up (ENU) direction, then the conversion matrix is expressed as follows:

$$T = \begin{bmatrix} q_0^2 + q_1^2 - q_2^2 - q_3^2 & 2(q_1q_2 - q_0q_3) & 2(q_1q_3 + q_0q_2) \\ 2(q_1q_2 + q_0q_3) & q_0^2 - q_1^2 + q_2^2 - q_3^2 & 2(q_2q_3 - q_0q_1) \\ 2(q_1q_3 - q_0q_2) & 2(q_2q_3 + q_0q_1) & q_0^2 - q_1^2 - q_2^2 + q_3^2 \end{bmatrix} \quad (11)$$

The heading angle is calculated as: $\varphi = arctan2(T_{12}, T_{22})$.

The heading angle calculated by CF and quaternion solution has high accuracy in a short time. However, the error gradually accumulates with time, so that the accuracy of trajectory calculation is seriously affected. The iHDE sets the dominant direction to eight, and corrects the heading angle towards the dominant direction to reduce the difference, but it is easy to overcorrect or fail to correct. Therefore, we propose an ADE model based on iHDE. Then the pedestrian walking states are divided into straight, turn and so on to correct respectively.

(1) Setting the dominant direction

During pedestrian walking, the maximum rotation of the pelvic cavity is between 4° −9°, and the smartphone will also produce a certain jitter. If the dominant direction is set to sixteen or more, the judgment conditions are harsh and difficult to achieve. Therefore, the dominant direction is set to eight, and the angle interval is 45° . The eight dominant directions are shown in Fig. 6.

(2) Judging the walking state

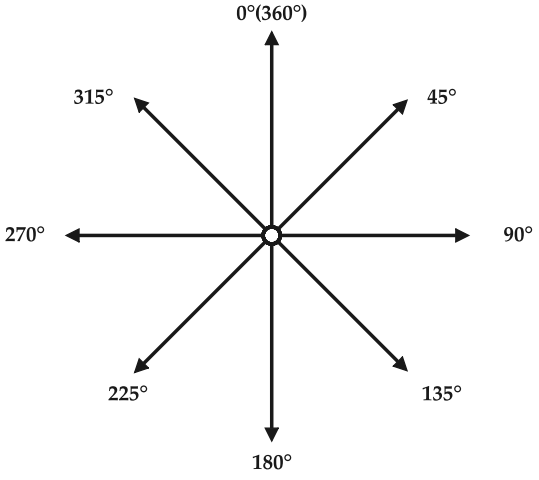

Fig. 6. The eight dominant directions.

In general case, the first two steps are identified as walking straight. Then starting from the third step, the current walking state is judged by using the continuous three steps heading:

$$Z = \begin{cases} 0 & (\varphi_i - \varphi_{i-1}) + (\varphi_{i-1} - \varphi_{i-2}) < 20 \\ 1 & otherwise \end{cases}, i = 3, 4, 5 \cdots end \quad (12)$$

Where φ_i represents the current step heading angle; φ_{i-1} represents the heading angle before one step; φ_{i-2} represents the heading angle before two steps. When $Z = 0$, the pedestrian is walking straight, and when $Z = 1$, the pedestrian is turning.

(3) Heading correction

According to the pedestrian walking state, the correction model is established in three types:

- When $Z_i = 1$, the pedestrian walking state is turning: The heading deviation is expressed as follows:

$$\Delta\varphi_i = mod(\varphi_i, 45) \quad (13)$$

Fig. 7. Three different performance smartphones.

Fig. 8. Three experimenters with different heights and genders.

Table 3
Smartphone built-in sensor parameters.

Smartphone brand	Sensor brand	Range	Noise density
XIAOMI 11 Pro	LSM6SDO Acc	±8 g	70 mg/$\sqrt{\text{Hz}}$
	LSM6SDO Gyro	±2000 mdp	3.8 mdps/$\sqrt{\text{Hz}}$
HUAWEI Enjoy 10 Plus	LSM6DS3-C Acc	±16 g	/
	LSM6DS3-C Gyro	±2000 mdp	/
HUAWEI MATE 30	ICM-20690 Acc	±16 g	100 ug/$\sqrt{\text{Hz}}$
	ICM-20690 Gyro	±2000 mdp	4 mdps/$\sqrt{\text{Hz}}$

Where mod represents the remainder function. The heading is corrected as follows:

$$\varphi_i = \begin{cases} \varphi_i - \Delta\varphi_i + 45 & \Delta\varphi_i > 22.5 \\ \varphi_i - \Delta\varphi_i & otherwise \end{cases} \tag{14}$$

- When $Z_i = 0$, $Z_{i-1} = 0$, the pedestrian walking state is walking straight:
  The heading deviation is expressed as follows:

$$\Delta\varphi_i = \varphi_i - 22.5 * round(\varphi_i/22.5) \tag{15}$$

Where round represents the floor function. The heading is corrected as follows:

$$\varphi_i = \varphi_i - \Delta\varphi_i - \Delta\varphi_i * sin\Delta\varphi_i * round(C_i/22.5) \tag{16}$$

- When $Z_i = 0$, $Z_{i-1} = 1$, the pedestrian walking state changes from turning to walking straight: The heading deviation is calculated with Eq. (14). The heading is corrected as follows:

$$\varphi_m = \begin{cases} \varphi_m - \Delta\varphi_i + 45 & \Delta\varphi_i > 22.5 \\ \varphi_m - \Delta\varphi_i & otherwise \end{cases}, m = i, i+1, i+2 \cdots end \tag{17}$$

Then the current point is corrected again, and the process is the same as Eqs. (16) and (17).

4. Experimental results and analysis

4.1. Experimental setup

In order to evaluate the adaptability of the PDR algorithm based on TCSLE and ADE models, three experimenters (as shown in Fig. 7) hold three smartphones with different performance: XIAOMI 11 Pro, HUAWEI Enjoy 10 Plus, HUAWEI MATE 30 (as shown in Fig. 8). Then the smartphone built-in sensor parameters are shown in Table 3. The body parameters of each experimenter are shown in Table 4.

The experiment factors are shown in Table 5. The experiment place is selected in the third-floor corridor of the Huihe Building of Liaoning Technical University. As shown in Fig. 9(a), The two paths are from A to D and from D to A respectively. The pedestrian walking pattern is walking smoothly with the hand-held smartphone, as shown in Fig. 9(b). The step uses the single-step count. In other words, the pedestrian lifts one foot off the ground, moves to a new position, and then puts it back to the ground as a step. The action decomposition is shown in Fig. 9(c).

Table 4
The experimenters' body parameters.

Experimenters	Sex	Height (m)	Average steplength (m)
Experimenter 1	Male	173	0.601
Experimenter 2	Female	161	0.527
Experimenter 3	Male	187	0.782

Table 5
The factors of experiment.

Experimenters	Smartphone brand	Route
Experimenter 1	XIAOMI 11 Pro	A-B-C-D
Experimenter 2	HUAWEI Enjoy 10 Plus	
Experimenter 3	HUAWEI MATE 30	D-C-B-A

4.2. Performance analysis of three-steps constriant step length estimation model

The Weinberg model and the single-step constraint step length estimation [45] are used as comparison experiments. In this paper, the step-length deviation Dev is used to evaluate the accuracy of TCSLE model:

$$Dev = \frac{|L - l|}{L} \tag{18}$$

Where L represents the actual step length; l represents the experimental step length.

The step-length average deviations of the TCSLE model and the comparison experiments are shown in Fig. 10. Using Matlab visualization, the step-length deviation curves are shown in Figs. 11–13.

It can be seen from Figs. 9 and 10 that the TCSLE model proposed in this paper has the best effect, and the average deviation of step length estimation is 1.0433%. The effect of single-step constraint step length estimation is second, the average deviation is 1.7908%. The Weinberg model has the worst step length estimation effect, and the average deviation of step length estimation is 2.7067%.

In summary, we systematically compare the proposed algorithm with the comparison algorithm, and the summary table of step-length deviation is shown in Table 6.

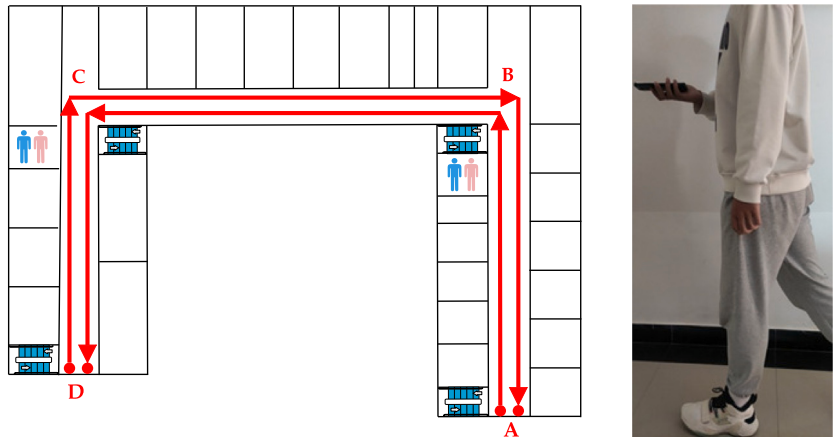

(a) Experimental place (b) Walking pattern

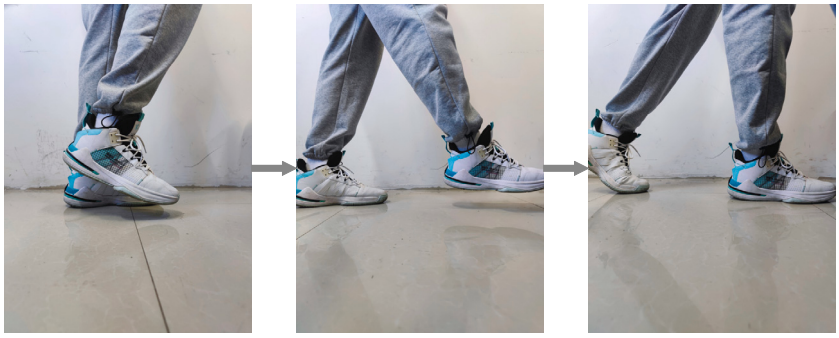

(c) Action decomposition

Fig. 9. The experimental designs.

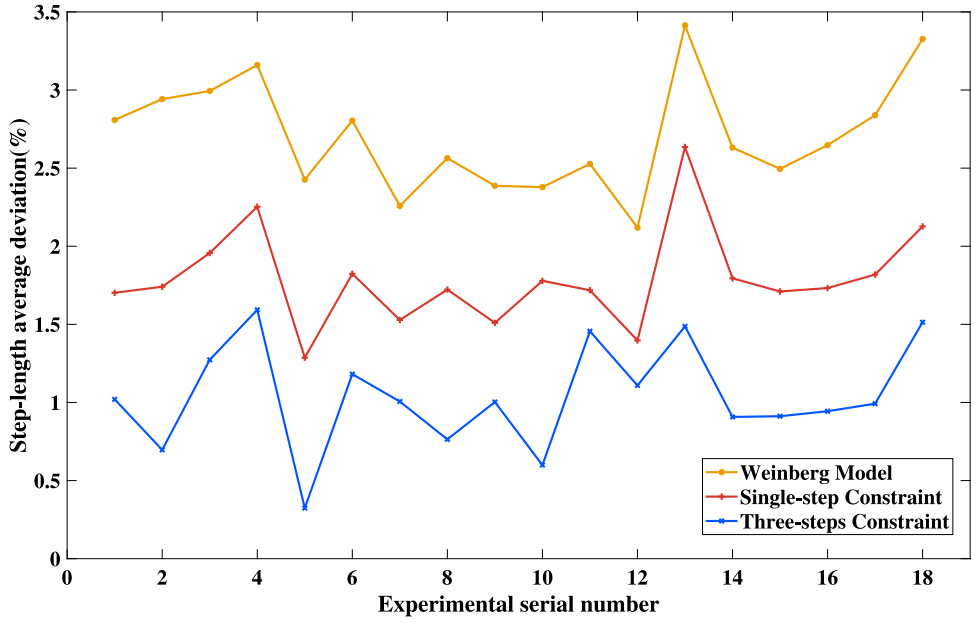

Fig. 10. The step-length average deviation curves.

4.3. Results of the proposed PDR algorithm

In Section 4.2, it has been determined that the TCSLE model work best. In order to further determine the performance of ADE, we introduce three comparison algorithms : electronic compass output, CF and iHDE. Then 18 sets of experimental results are compared.

We evaluate the algorithm accuracy by calculating the relative positioning error Rpe between the experiment and real end point

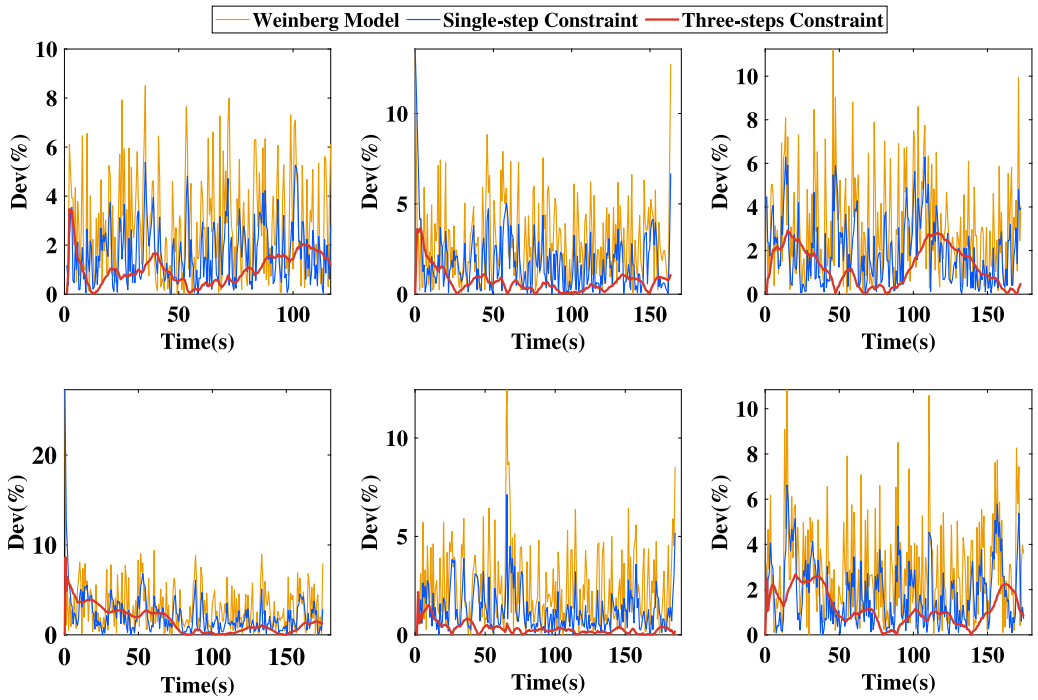

Fig. 11. The step-length deviation curves of Experimenter 1.

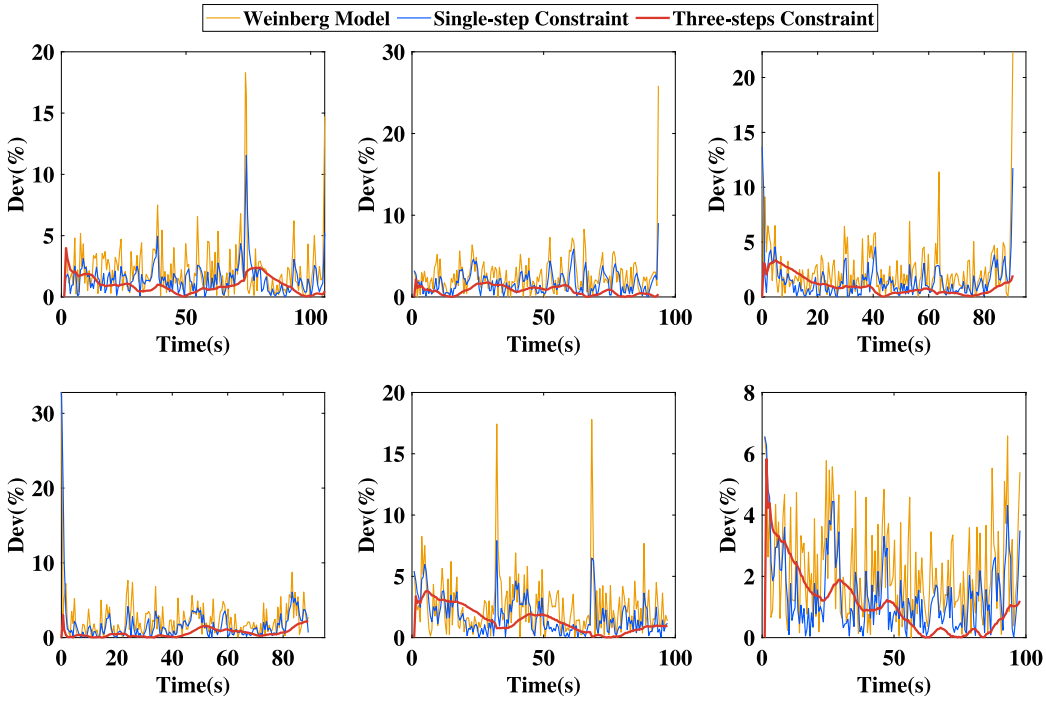

Fig. 12. The step-length deviation curves of Experimenter 2.

Table 6
The summary table of step-length deviation.

Deviation	Weinberg model	Single-step constraint	Three-steps constraint
Maximum(%)	3.4136	2.6351	1.4871
Average(%)	2.7067	1.7908	1.0433

coordinates:

$$Hpe = \sqrt{(X - x)^2 + (Y - y)^2} \tag{19}$$

$$Rpe = \frac{Hpe}{Lsum} \tag{20}$$

Where Hpe represents the horizontal positioning error; (X, Y) represents the real endpoint coordinate; (x, y) represents the experiment endpoint coordinate; $Lsum$ represents the total length of the experimental route.

The relative positioning errors of pedestrian trajectory are shown in Fig. 14 . The pedestrian trajectories are shown in Figs. 15 -17.

It can be seen from Figs. 14–17 that:

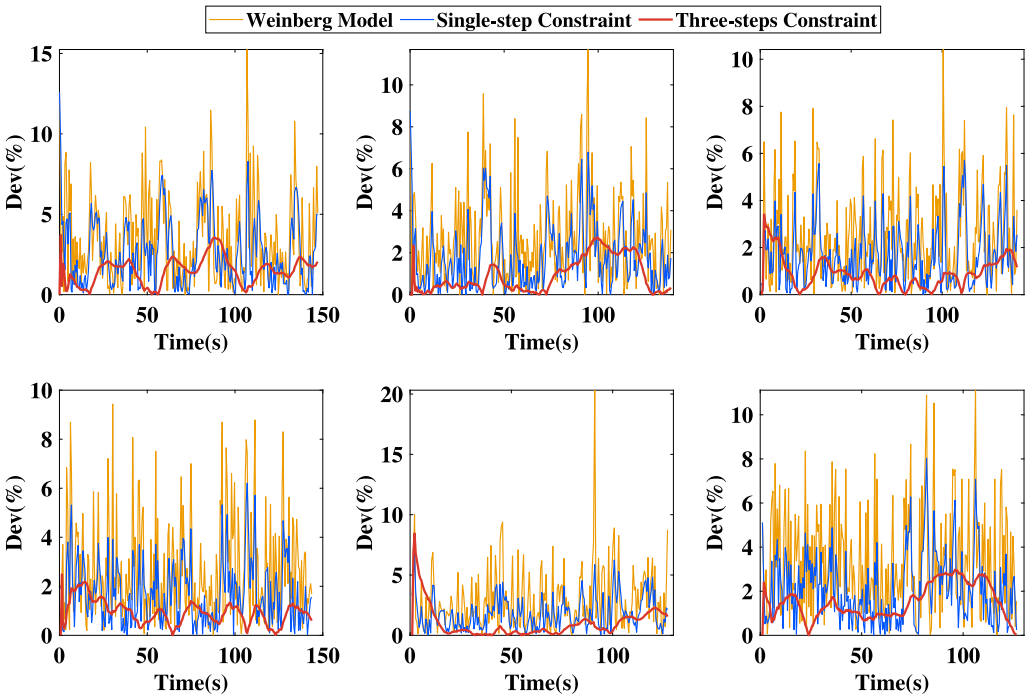

Fig. 13. The step-length deviation curves of Experimenter 3.

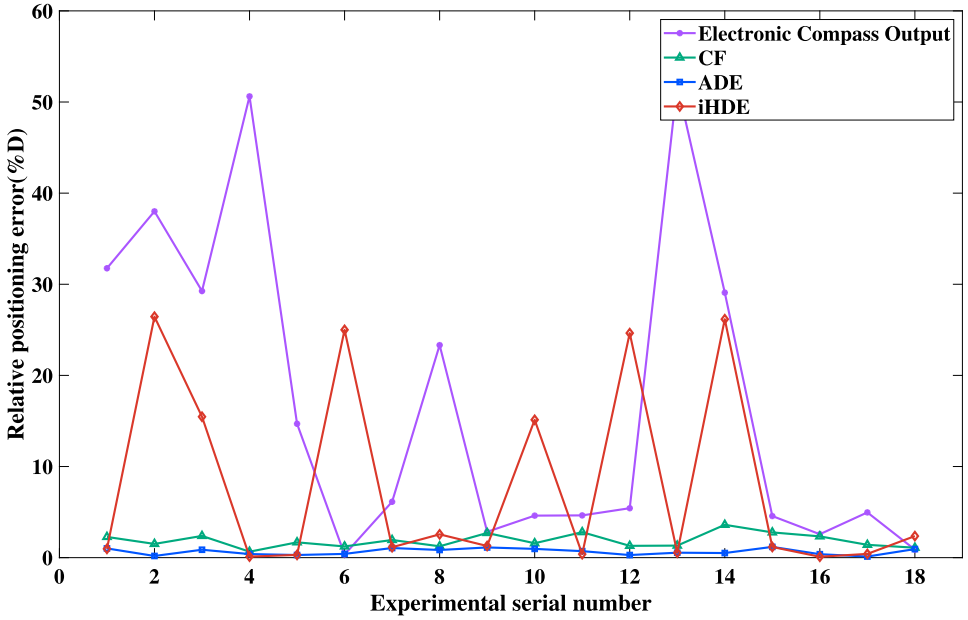

Fig. 14. The relative positioning error curves.

The heading angle obtained by electronic compass output is not stable. The average horizontal positioning error is 23.0895 m, and the average relative positioning error is 16.9776 %D. The two errors are far bigger than the other two models. Then the heading angle obtained by CF has a small offset. The horizontal positioning error of pedestrian trajectory is concentrated in one to three meters. The average horizontal positioning error is 16.9776 m, and the average relative positioning error is 16.9776 %D. Then the heading angle obtained by iHDE has poor robustness, but the accuracy of most experiments is good. However, in general, the average horizontal positioning error is 16.9776 m, and the average relative positioning error is 16.9776 %D. Finally, the heading angle obtained by ADE is very stable. The horizontal positioning error of pedestrian trajectory is concentrated in about one meter. The average horizontal positioning error is 0.8923 m, and the average relative positioning error is 16.9776 %D. Thus, the proposed algorithm has a more accurate indoor positioning effect.

In summary, we systematically compare the proposed algorithm with the comparison algorithm, and the summary table of relative positioning error is shown in Table 7.

5. Conclusions

Aiming at the problem of fast accumulation and divergence of pedestrian trajectory error caused by the zero-bias instability of smartphone built-in MEMS sensors, We propose a PDR algorithm based on TCSLE and ADE models. The algorithm uses bias drift and KF to denoise

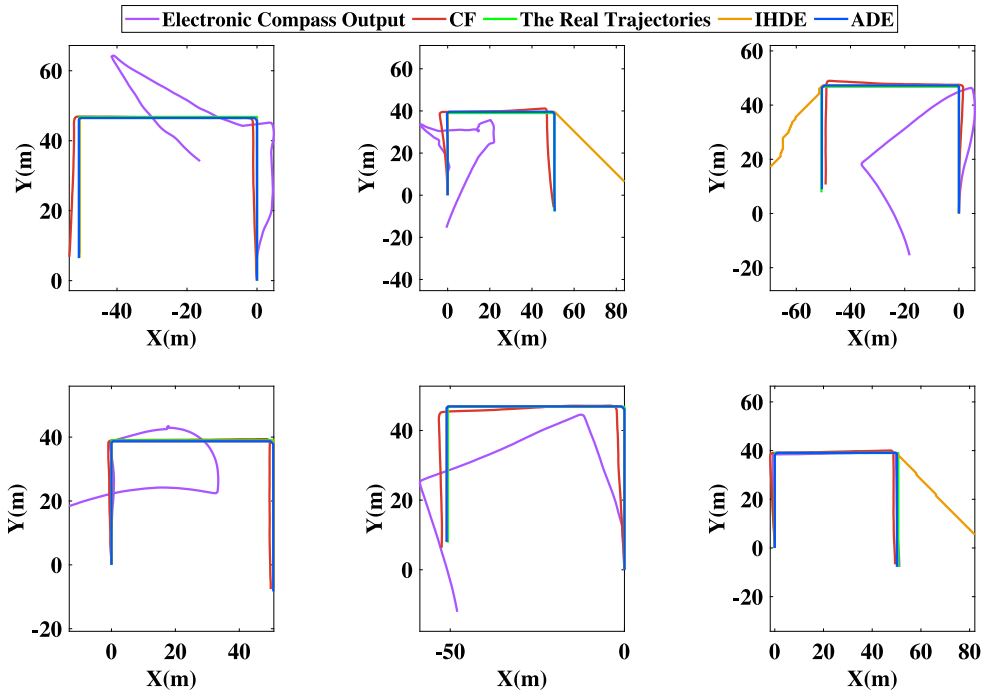

Fig. 15. The pedestrian trajectories of Experimenter 1.

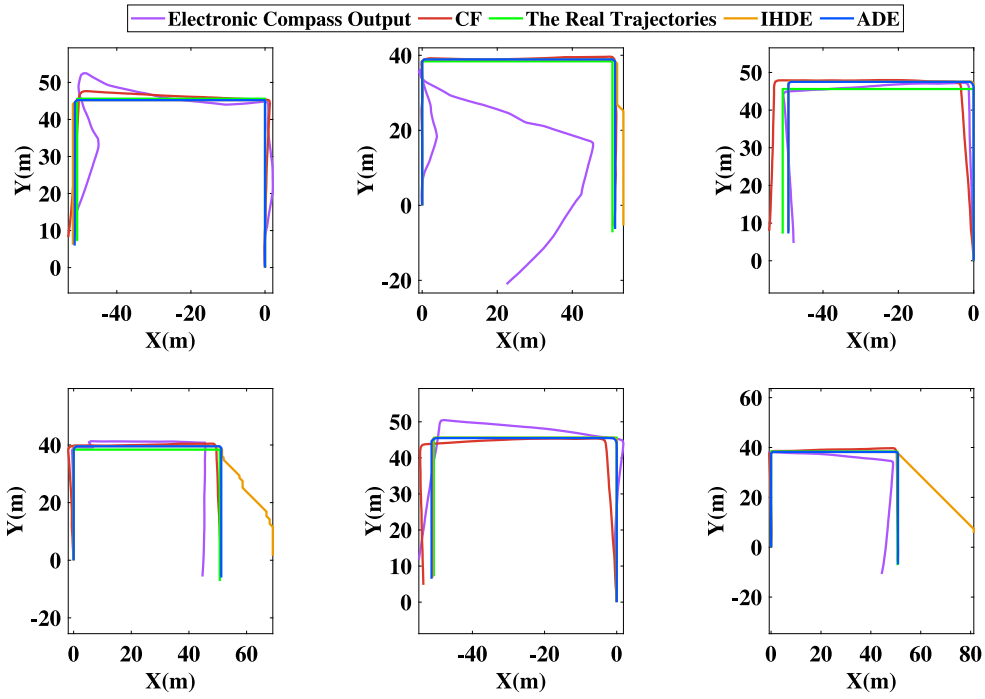

Fig. 16. The pedestrian trajectories of Experimenter 2.

the original data, and constructs the peak domain and time domain to detect pedestrian step information. The TCSLE and ADE models are proposed to improve the calculation accuracy of step length and heading, then the accurate step length and heading information are detected, respectively. Finally, the pedestrian trajectory is reconstructed by using the step length and heading information. In order to evaluate the performance of the proposed algorithm, Three experimenters held three different types of smartphones to move smoothly along two paths at a constant speed, and a total of 18 experiments were conducted. The experimental results show that compared with the comparison test, the step length deviation of the proposed algorithm is reduced by 0.2627 % to 2.2454 %, the horizontal positioning error is reduced by 0.0133 m to 69.8418 m, and the relative positioning error is reduced by 0.0098 %D to 51.3543 %D. In general, the step length deviation of the proposed algorithm is less than 1.4871 %, the horizontal positioning error is less than 1.6070 m, and the relative positioning error is less than 1.1816 %D. It has strong adaptability and robustness, and the indoor positioning effect is more accurate. However, the algorithm proposed

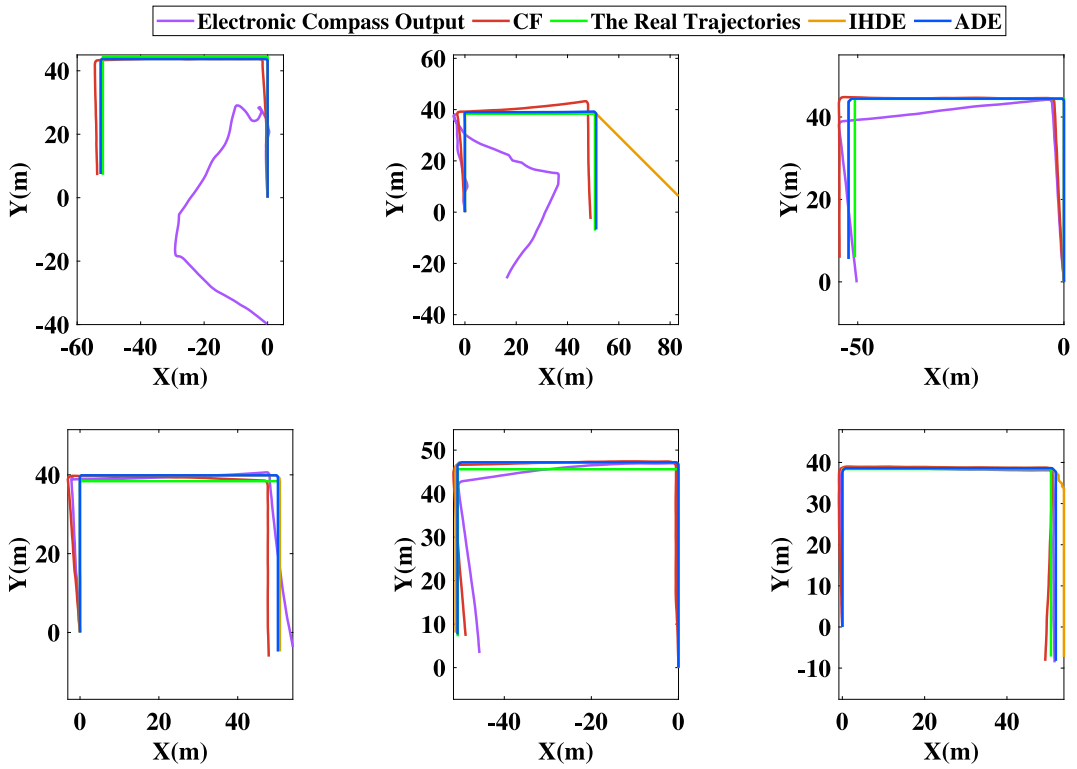

Fig. 17. The pedestrian trajectories of Experimenter 3.

Table 7
The summary table of relative positioning error.

Error		Electronic compass output	CF	iHDE	ADE
Hpe(m)	Maximum	68.8454	3.8065	1.6070	35.9652
	Average	23.0895	2,5554	0.8922	10.8936
Rpe(%D)	Maximum	50.6216	2.7989	1.1816	26.4450
	Average	16.9776	1.8790	0.6561	8.0100

in this paper is only limited to the trajectory reconstruction of the two-dimensional plane. In reality, the pedestrian cannot be confined to a certain floor. In the future, we plan to add information such as air pressure to this algorithm, extend it to three-dimensional space, and apply it to smart city construction. Secondly, the algorithm proposed in this paper is based on the situation that pedestrians walk at a constant speed. In reality, the situation is complicated when pedestrians walk. In the future, we plan to add intelligent algorithms to this algorithm to intelligently identify pedestrian walking status.

Declaration of competing interest

The authors declare that they have no known competing financial interests or personal relationships that could have appeared to influence the work reported in this paper.

Data availability

Data will be made available on request.

Acknowledgments

This research was supported by Liaoning Provincial Department of Education Project (No. LJ2020JCL015) and State Key Laboratory of Geo-Information Engineering and Key Laboratory of Surveying and Mapping Science and Geospatial Information Technology of MNR, CASM (NO.2022-01-11).

References

[1] Bi J. Study on optimization problem of Wi-Fi/PDR indoor hybrid positioning on smartphone. Acta Geod Et Cartogr Sin 2021;50(10):1416.
[2] Kuang J, Ge W, Zhang Q, Dou Z, Tang A, Zhang X, et al. Smartphone built-in sensors based vehicle integrated positioning method. J Tradit Chin Med 2020;28(06):701–8.
[3] Yu Y, Chen R, Chen L, Xu S, Li W, Wu Y, et al. Precise 3-D indoor localization based on Wi-Fi FTM and built-in sensors. IEEE Internet Things J 2020;7(12):11753–65.
[4] Yu Y, Chen R, Shi W, Chen L. Precise 3D indoor localization and trajectory 0ptimization based on sparse Wi-Fi FTM anchors and built-in sensors.2022. IEEE Trans Veh Technol 2020;71(4):4042–56.
[5] Jiang C, Chen Y, Xu B. Vector tracking based on factor graph optimization for GNSS NLOS bias estimation and correction. IEEE Internet Things J 2022;1.
[6] Zhou R, Luo L, Li Z. An indoor pedestrian positioning algorithm based on smartphone sensor. Comput. Eng. 2016;42(11):22–6.
[7] Li X. GNSS repeater based differential indoor positioning with multi-epoch measurements. IEEE Trans Intell Veh. 2023;8(1):803–13.
[8] Li X, Wei D, Lai Q, Xu Y, Yuan H. Smartphone-based integrated PDR/GPS/Bluetooth pedestrian location. Adv Space Res 2017;59(3):877–87.
[9] Yan K, Chen R, Guo G, Chen L. Locating smartphone indoors by using tightly coupling bluetooth ranging and accelerometer measurements. Remote Sens 2022;14:3468.
[10] Ye F, Chen R, Guo G, Peng X, Liu Z, Huang L. A low-cost single-anchor solution for indoor positioning using BLE and inertial sensor data. IEEE Access 2019;7:162439–53.
[11] Chen J, Song S, Yu H. An indoor multi-source fusion positioning approach based on PDR/MM/WiFi. Int J Electron Commun (AEU) 2021;135:153733.
[12] Li Y, Zhuang Y, Lan H, Zhang P, Niu X, El-Sheimy N. WiFi-aided magnetic matching for indoor navigation with consumer portable devices. Micromachines 2015;6:747–64.
[13] Guo G, Chen R, Ye F, Peng X, Liu Z, Pan Y. Indoor smartphone localization: a hybrid WiFi RTT-RSS ranging approach. IEEE Access 2019;7:176767–81.
[14] Kuang J, Niu X, Zhang P, Chen X. Indoor positioning based on pedestrian dead reckoning and magnetic field matching for smartphones. Sensors 2018;18:4142.
[15] Cho H, Kmon Y. RSS-based indoor localization with PDR location tracking for wireless sensor networks. Int J Electron Commun (AEU) 2016;70(3):250–6.
[16] Xu H, Wu M, Li P, Zhu F, Wang R. An RFID indoor positioning algorithm based on support vector regression. Sensors 2018;18:1504.
[17] Huang X, Xiong Z, Xu J. Research on pedestrian navigation algorithm based on zero velocity update/heading error self-observation/geomagnetic matching. Acta Armamentarii 2017;38(10):2031–40.

[18] Zhu J, Wang L, Bo Y. Pedestrian GNSS/PDR integrated navigation system with graph optimization. Acta Armamentarii. http://kns.cnki.net/kcms/detail/11.2176.TJ.20221212.1818.002.html.
[19] Sun R, Zhang Z, Cheng Q. Pseudorange error prediction for adaptive tightly coupled GNSS/IMU navigation in urban areas. GPS Solut 2022;26(1):1–13.
[20] Fang X, Tao T, Li J, He H, Feng J. Research on heading estimation algorithm based on mobile phone inertial sensors. Transducer Microsyst Technol 2020;39(05):17–20.
[21] Zhang X, Luo K, Tao X, Hu X, Liu W. A multi-mounted PDR algorithm based on wearable MEMS sensors state recognition. Geomat. Inf. Sci. Wuhan Univ. 2021;46(12):1791–801.
[22] Yamagishi S, Jing L. Pedestrian dead reckoning with low-cost foot-mounted IMU sensor. Micromachines 2022;13:610.
[23] Zhou Z, Feng W, Li P, Liu Z, Xu X, Yao Y. A fusion method of pedestrian dead reckoning and pseudo indoor plan based on conditional random field. Measurement 2023;207:112417.
[24] Xie D, Jiang J, Wu J, Yan P, Tang Y, Zhang C, et al. A robust GNSS/PDR integration scheme with GRU-based zero-velocity detection for mass-pedestrians. Remote Sens 2022;14:300.
[25] Ju H, Park C. A pedestrian dead reckoning system using a foot kinematic constraint and shoe modeling for various motions. Sensors Actuators A 2018;284:135–44.
[26] Wu B, Ma C, Poslad S, Selviah DR. An adaptive human activity-aided hand-held smartphone-based pedestrian dead reckoning positioning system. Remote Sens 2021;13:2137.
[27] Chen R, Guo G, Ye F, Qian L, Xu S, Li Z. Tightly-coupled integration of acoustic signal and MEMS sensors on smartphones for indoor positioning. Acta Geod Et Cartogr Sin 2021;50(02):143–52.
[28] Jing T, Zhao H. Research on array MEMS inertial sensors and noise suppression. Chin J Sens Actuators 2020;33(06):779–84.
[29] Li X, Yuan H, Yang G, Gong Y, Xu J. A novel algorithm for scenario recognition based on MEMS sensors of smartphone. Micromachines 2022;13:1865.
[30] Xu Y, Gao L, Wang F, Wang R. Personal positioning method based on the step length estimation model improved by the surface EMG signal. J Tradit Chin Med 2022;30(01):15–21.
[31] Yao Y, Pan L, Feng W, Xu X, Liang X, Xu X. A robust step detection and stride length estimation for pedestrian dead reckoning using a smartphone. IEEE Sens J 2020;20(17):9685–97.
[32] Hannink J, Kautz T, Pasluosta C, Barth J, Schülein S, Gabmann KG, et al. Mobile stride length estimation with deep convolutional neural networks. IEEE J Biomed Health Inform 2018;22:354–62.
[33] Vezočnik M, Kamnik R, Juric MB. Inertial sensor-based step length estimation model by means of principal component analysis. Sensors 2021;21:3527.
[34] Zhang H, XU X, Dai R. Indoor personal navigation algorithms based on the MEMS and android smartphone. J Beijing Univ Technol 2017;43(05):729–35.
[35] Wang P, Z. Meng, Deng Z. Research on heuristic heading compensation algorithm with buffers in waist-mounted pedestrian navigation system. Navig Position Timing 2020;7(03):150–6.
[36] Hu G, Wan H, Li X. A high-precision magnetic-assisted heading angle calculation method based on a 1D convolutional neural network (CNN) in a complicated magnetic environment. Micromachines 2020;11:642.
[37] Wagstaff B, Kelly J. LSTM-based zero-velocity detection for robust inertial navigation. In: Proceedings of the 2018 international conference on indoor positioning and indoor navigation , vol. 24–27. 2018, p. 1–8.
[38] Deng P, Zhu F, Zhao R. An indoor inertial navigation and positioning algorithm based on accurate heading angle correction. J. Chin Inert Technol 2020;28(06):716–22.
[39] Yan G, Li Z, Zhu H. Gyroscope drift error identification and reconstruction based on allan variance analysis. J. Navig Position 2022;10(04):29–33.
[40] Li J, Fu J, Li Z, Yang J. Random noise analysis of MEMS inertial devices based on allan variance method. Sens World 2021;27(10):31–5.
[41] Ma Q, Wang Q, Yang Y, Sheng H. Random error identification and suppression of MEMS gyroscope based on allan variance. Trans Microsyst Technol 2019;38(06):62–5.
[42] Liu C, Kadja T, Chodavarapu VP. Experimental evaluation of sensor fusion of low-cost UWB and IMU for localization under indoor dynamic testing conditions. Sensors 2022;22:8156.
[43] Li H, Guo H, Qi Y, Deng L, Yu M. Research on multi-sensor pedestrian dead reckoning method with UKF algorithm. Measurement 2021;169:108524.
[44] Basso M, Martinelli A, Morosi S, Sera F. A real-time GNSS/PDR navigation system for mobile devices. Remote Sens 2021;13:1567.
[45] Zhou Y. Research on indoor location based on smart phone and PDR [Master's thesis], Hangzhou: Zhejiang Gongshang University; 2020.